





## Stability of a thin viscoelastic film falling down an inclined plane

Tao Hu, Qing-fei Fu , Yan Xing, and Li-jun Yang \*

*School of Astronautics, Beihang University, Beijing 100083, China*

Luo Xie 

*School of Marine Science and Technology, Northwestern Polytechnical University,  
Xi' an, Shaanxi 710072, China*

 (Received 7 February 2021; accepted 6 July 2021; published 12 August 2021)

The stability of a thin viscoelastic film of Oldroyd-B fluid falling down an incline is investigated. In the weak viscoelasticity limit, a reduced model is derived using the weighted residual techniques, which consists of two coupled equations for the film thickness and local flow rate. Through the normal mode analysis, temporal growth rates and neutral stability curves are calculated to explore linear stability of the film. Results show that the viscoelasticity acts to destabilize the film and decrease the phase speed of linear waves. Good agreement is found between the reduced model and full linearized equations solved by the Chebyshev spectral collocation method when viscoelastic effect is relatively weak. Nonlinear traveling waves are further determined. The speed of fast/slow-wave families is promoted/reduced in the presence of the viscoelasticity, resulting in a dispersion effect on the system; while the wave amplitudes are augmented for both fast and slow waves. Besides, the temporal evolution of surface waves is numerically resolved, which validates the linear prediction of the instability threshold. Steady permanent waves are observed in the final stage; the surface deformation and perturbation energy are enhanced by the viscoelasticity as expected.

DOI: [10.1103/PhysRevFluids.6.083902](https://doi.org/10.1103/PhysRevFluids.6.083902)

### I. INTRODUCTION

Falling liquid films are encountered in various industrial fields like heat and mass exchangers [1], coating processes [2], and cooling systems of combustion chamber in rocket engines [3], as well as daily life. As a result, much work has been done on the hydrodynamic instability problem of falling films in the past decades [4–7]. Early researches were initiated by the experiment of Kapitza and Kapitza [8] where the well-known long-wave instability of thin films flowing down an incline is observed. Benjamin [9] and Yih [10] carried out theoretical studies and concluded that the critical Reynolds number for the onset of this instability depends on the inclination of the plane. A significant experimental work is later conducted by Liu *et al.* [11], where they confirmed the prediction of the instability threshold and showed the convective nature of the film instability. Smith [12] proposed a detailed explanation on the instability mechanism where the inertia is claimed to play a key role.

Over the years, several models have been devised to account for the dynamics of falling films [13]. Applying a long-wave expansion technique, Benney [14] first derived a single evolution equation of the film thickness  $h$ , which proved to be effective in capturing the instability threshold. However, as pointed out by Pumir *et al.* [15], Benney equation (BE) suffers from unphysical finite-time blow-up which thus limits its validity at larger Reynolds numbers beyond the criticality.

---

\*yanglijun@buaa.edu.cn

One remedy for this drawback is the integral boundary layer (IBL) model derived by Shkadov [16], who introduced the local flow rate  $q$  as an additional degree of freedom to the system. Though IBL is able to describe the film flow at moderate Reynolds numbers, it fails to determine accurately the instability threshold [7]. To fix this defect, Ruyer-Quil and Manneville [17,18] employed a weighted residual technique and obtained a series of reduced equations, which are often referred to as the weighted residual integral boundary layer (WRIBL) model. And this approach has later been commonly adopted to investigate thin film flows because of its relatively good performance in both linear and nonlinear regimes [19–23].

On the other hand, in many engineering applications the working fluid is viscoelastic, which thus inspired some research interest in the film flow of the viscoelastic fluids [24,25]. Gupta [26] studied the linear stability of a second-order viscoelastic film and concluded that the viscoelasticity destabilizes the film. Shaqfeh *et al.* [27] analyzed the Oldroyd-B fluid film and also observed destabilizing impact of the viscoelasticity at small Reynolds numbers, which agreed with previous researches [28,29]; while the a primarily stabilizing effect of the elasticity for moderate Reynolds numbers was also pointed out. Specially, a purely elastic instability was identified for sufficiently large Deborah numbers. Joo [30] considered the film flow utilizing a four-constant Oldroyd model which incorporates both the elastic and shear-thinning effect. Following a long-wave expansion procedure, Kang and Chen [31] obtained a second-order evolution equation for Oldroyd-B film and analyzed the nonlinear waves resulting from the elastic instability. Tihon and Wein [32] conducted an experiment on viscoelastic film flows and confirmed the destabilizing impact of the fluid viscoelasticity. Besides, they also observed elastic instabilities in small inclination angles. Andersson and Dahl [33] investigated the steady laminar film flow of Walters' liquid B'' and showed that viscoelastic films develop more rapidly towards the downstream traveling-wave state than Newtonian counterparts. And the influence of evaporation and bottom heating were also considered for Walters B'' films [34].

Saprykin *et al.* [35] extended IBL model for viscoelastic film flowing over topography by assuming weak topography and viscoelasticity. A second-order two-equation model is employed by Amatoousse *et al.* [36] to investigate the stability of a falling Walters B'' film. And they discussed the bifurcation behavior and nonlinear development of the traveling waves on the free surface. Davalos-Orozco [37] derived a Benney-type equation for an Oldroyd-B film flowing down a wavy wall and showed that a spatial resonant effect due to the waviness of the wall is possible to passively stabilize the viscoelastic film. Recently, Sharma *et al.* [38] revisited the problem and solved the linear instability using Floquet theory whereby the elastic instability was divided into three regimes according to the wall wavelength. Moreover, simulations of the evolution equation indicated the existence of several nonlinear states like the traveling waves, time-periodic waves, and chaos. Pettas *et al.* [39,40] also considered the viscoelastic film which obeys the Phan-Thien-Tanner constitutive model flowing down an inclined wall with sinusoidal corrugations. The steady-state flow was determined by numerical calculations based on the finite-element method while the linear stability problem was resolved using Floquet-Bloch theory. Their results demonstrated that three-dimensional instability may arise for highly elastic fluids.

In this paper, instead of BE and IBL adopted in previous studies, we make an effort to employ the WRIBL model to investigate the viscoelastic film flow in both linear and nonlinear region, which has not been clearly clarified yet. Section II presents the governing equation based on which a reduced model is derived for the film flow. In Sec. III we examine the linear stability using both the reduced model and full equations. Nonlinear traveling waves are obtained and discussed in Sec. IV. Moreover, numerical simulations of model equations are performed in Sec. V and the conclusions are drawn in Sec. VI.

## II. MATHEMATICAL FORMULATION

### A. Governing equations

Consider a thin viscoelastic film with density  $\rho$  and surface tension  $\sigma$  flowing down a plane inclined at the angle  $\theta$ , as depicted in Fig. 1. We introduce a Cartesian coordinate  $(x, y)$  with  $x$

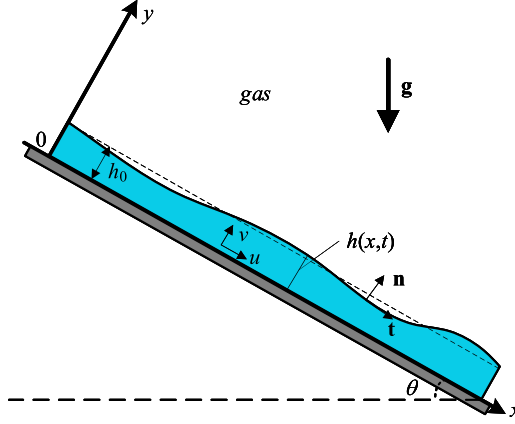


FIG. 1. Schematic of a thin film flowing down an incline.

pointing toward the streamwise direction and  $y$  denoting the outward cross-stream direction. The mass and momentum equations in the fluid layer are given by

$$\nabla \cdot \mathbf{u} = 0, \quad (1)$$

$$\rho(\partial_t \mathbf{u} + \mathbf{u} \cdot \nabla \mathbf{u}) = -\nabla p + \nabla \cdot \boldsymbol{\tau} + \rho \mathbf{g}, \quad (2)$$

where  $\mathbf{u} = (u, v)$  is the velocity vector,  $\nabla = (\partial_x, \partial_y)$  is the gradient operator on the  $(x, y)$  plane and  $\mathbf{g} = (g \sin \theta, -g \cos \theta)$  represents the gravitational acceleration. For the stress tensor  $\boldsymbol{\tau}$ , we adopt the Oldroyd-B constitutive model, which is an appropriate approximation for a Boger fluid (an elastic liquid with a constant viscosity) under relatively small shear rates [41]; and it has been frequently used to study the unsteady shear flows with viscoelastic effects. Oldroyd-B equation is written as

$$\boldsymbol{\tau} + \lambda_1 \mathcal{L} \boldsymbol{\tau} = 2\mu(\mathbf{D} + \lambda_2 \mathcal{L} \mathbf{D}), \quad (3)$$

where  $\mathbf{D} = [(\nabla \mathbf{u}) + (\nabla \mathbf{u})^T]/2$  is the rate-of-strain tensor,  $\lambda_1$  is the stress relaxation time and  $\lambda_2$  is deformation retardation time of the fluid. The operator  $\mathcal{L}$  denotes the upper convected derivative

$$\mathcal{L} \boldsymbol{\tau} = \partial_t \boldsymbol{\tau} + \mathbf{u} \cdot \nabla \boldsymbol{\tau} - (\nabla \mathbf{u}) \cdot \boldsymbol{\tau} - \boldsymbol{\tau} \cdot (\nabla \mathbf{u})^T. \quad (4)$$

In the limit case  $\lambda_2 = 0$ , Eq. (3) corresponds to a upper convected Maxwell fluid; and a purely Newtonian fluid is recovered when further letting  $\lambda_1 = 0$ .

On the bottom plane we have the no-slip boundary condition

$$\mathbf{u} = 0 \quad \text{at} \quad y = 0. \quad (5)$$

At the free surface  $y = h(x, t)$  the film satisfies the kinematic condition

$$v = \partial_t h + u \partial_x h, \quad (6)$$

together with the normal and tangential stress balances

$$p - p_g + \mathbf{n} \cdot \boldsymbol{\tau} \cdot \mathbf{n} = \sigma(\nabla \cdot \mathbf{n}), \quad (7)$$

$$\mathbf{n} \cdot \boldsymbol{\tau} \cdot \mathbf{t} = 0. \quad (8)$$

Here,  $\mathbf{n}$  and  $\mathbf{t}$  is the unit normal and tangential vector at the interface

$$\mathbf{n} = \frac{1}{n}(-\partial_x h, 1), \quad \mathbf{t} = \frac{1}{n}(1, \partial_x h), \quad n = \sqrt{1 + (\partial_x h)^2}, \quad (9)$$

respectively.

The parallel basic state solution of the above system Eqs. (1)–(9) can be easily determined:

$$\begin{aligned}\bar{u} &= \frac{\rho g \sin \theta h_0^2}{2\mu}(2y - y^2), \quad \bar{v} = 0, \quad \bar{p} = \rho g \cos \theta (h_0 - y) + p_g, \\ \bar{\tau}_{xx} &= 2\mu(\lambda_1 - \lambda_2)(\partial_y \bar{u})^2, \quad \bar{\tau}_{xy} = \mu \partial_y \bar{u}, \quad \bar{\tau}_{yy} = 0,\end{aligned}\quad (10)$$

where  $h_0$  is the uniform layer thickness of the film. Then we apply the following scaling procedure to above equations:

$$\begin{aligned}(x, y) &= (lx^*, h_0 y^*), \quad (u, v) = u_0(u^*, \delta v^*), \quad h = h_0 h^*, \quad t = \frac{l}{u_0} t^*, \\ p - p_g &= \rho u_0^2 p^*, \quad (\tau_{xx}, \tau_{xy}, \tau_{yy}) = \frac{h_0}{\mu u_0} \left( \frac{1}{\delta} \tau_{xx}^*, \tau_{xy}^*, \delta \tau_{yy}^* \right),\end{aligned}\quad (11)$$

where  $u_0 = \rho g \sin \theta h_0^2 / (2\mu)$  is the average velocity of the basic flow. Note that we have introduced  $\delta = h_0/l \ll 1$  as a thin-film parameter with  $l$  being the length scale in the  $x$  direction. For the simplicity of the notation, we drop the superscript asterisks from all the dimensionless variables. Then the dimensionless governing equations of motion write

$$\partial_x u + \partial_y v = 0, \quad (12)$$

$$\delta \text{Re}(\partial_t u + u \partial_x u + v \partial_y u) = -\delta \text{Re} \partial_x p + \partial_x \tau_{xx} + \partial_y \tau_{xy} + 3, \quad (13)$$

$$\delta^2 \text{Re}(\partial_t v + u \partial_x v + v \partial_y v) = -\text{Re} \partial_y p + \delta(\partial_x \tau_{xy} + \partial_y \tau_{yy}) - 3 \cot \theta, \quad (14)$$

where  $\text{Re} = \rho u_0 h_0 / \mu$  is the Reynolds number. And the stress components are expressed by

$$\begin{aligned}\tau_{xx} + \delta De[\partial_t \tau_{xx} + u \partial_x \tau_{xx} + v \partial_y \tau_{xx} - 2(\tau_{xx} \partial_x u + \tau_{xy} \partial_y u)] \\ = 2\delta^2 \partial_x u + \delta r De[\delta^2(\partial_{xt} u + u \partial_{xx} u + v \partial_{xy} u) - (\partial_y u + \delta^2 \partial_x v) \partial_y u - 2\delta^2(\partial_x u)^2],\end{aligned}\quad (15)$$

$$\begin{aligned}\tau_{xy} + \delta De[\partial_t \tau_{xy} + u \partial_x \tau_{xy} + v \partial_y \tau_{xy} - (\tau_{xy} \partial_x u + \tau_{yy} \partial_y u) - (\tau_{xx} \partial_x v + \tau_{xy} \partial_y v)] \\ = \partial_y u + \delta^2 \partial_x v + \delta r De[\partial_{yt} u + \delta^2 \partial_{xt} v + u(\partial_{xy} u + \delta^2 \partial_{xx} v) \\ + v(\partial_{yy} u + \delta^2 \partial_{xy} v) + 2\partial_x u(\partial_y u - \delta^2 \partial_x v)],\end{aligned}\quad (16)$$

$$\begin{aligned}\tau_{yy} + \delta De[\partial_t \tau_{yy} + u \partial_x \tau_{yy} + v \partial_y \tau_{yy} - 2(\tau_{xy} \partial_x v + \tau_{yy} \partial_y v)] \\ = 2\{\partial_y v + \delta r De[\partial_{yt} v + u \partial_{xy} v + v \partial_{yy} v - (\partial_y u + \delta^2 \partial_x v) \partial_x v - 2(\partial_y v)^2]\},\end{aligned}\quad (17)$$

where  $De = \lambda_1 u_0 / h_0$  is the Deborah number and  $r = \lambda_2 / \lambda_1$  denotes the ratio of deformation retardation time to stress relaxation time (also referred to as the time constant ratio). And these equations are subjected to the no-slip boundary condition

$$u = 0, \quad v = 0, \quad \text{at } y = 0, \quad (18)$$

and the dimensionless kinematic and dynamic boundary conditions at the free surface  $y = h(x, t)$ ,

$$v = \partial_t h + u \partial_x h, \quad (19)$$

$$[1 - \delta^2(\partial_x h)^2] \tau_{xy} + \partial_x h(\delta^2 \tau_{yy} - \tau_{xx}) = 0, \quad (20)$$

$$p - \frac{\delta}{\text{Re}[1 + \delta^2(\partial_x h)^2]} \{(\partial_x h)^2 \tau_{xx} + \tau_{yy} - 2\tau_{xy} \partial_x h\} = -\frac{3\delta^2 We}{\text{Re}} \frac{\partial_{xx} h}{[1 + \delta^2(\partial_x h)^2]^{3/2}} \quad (21)$$

with  $We = \sigma / (\rho g h_0^2 \sin \theta)$  being the Weber number.

### B. Weighted residual integral boundary layer model

In what follows, a weighted residual technique is employed to derive a reduced model based on the above equations Eqs. (12)–(21), which has been frequently utilized in previous studies on falling films [19–23]. After neglecting all the terms of higher orders than  $O(\delta^2)$ , we assume a self-similar velocity profile in the fluid layer with

$$u = \frac{3q}{2h^3}b, \quad (22)$$

where  $b = y(2h - y)$  and  $q = \int_0^h u dy$  represents the flow rate. The prescribed profile for  $u$  satisfies the no-slip condition Eq. (18) and the free-surface condition Eq. (20) to  $O(\delta)$ . And as noted by Kalliadasis *et al.* [42], Eq. (20) is actually incorporated into the momentum equation (13) when it is integrated over the film thickness later.

In the present study, we adopt a weak viscoelasticity approximation with  $De \ll 1$  which enables us to obtain explicit expressions for the stresses and thus substantially simplify the formulation of the model. This assumption has been made by a number of authors when analyzing the thin-film flows of the viscoelastic fluids [35,43]. Therefore, evaluating Eqs. (15)–(17) the following approximation at first order in  $De$  for the stresses readily gives

$$\begin{aligned} \tau_{xx} = & 2\delta^2 \partial_x u - \delta De(1-r)[\delta^2(\partial_{xt}u + u\partial_{xx}u + v\partial_{xy}u) \\ & - (\partial_y u + \delta^2 \partial_x v)\partial_y u - 2\delta^2(\partial_x u)^2], \end{aligned} \quad (23)$$

$$\begin{aligned} \tau_{xy} = & \partial_y u + \delta^2 \partial_x v - \delta De(1-r)[\partial_{yt}u + \delta^2 \partial_{xt}v + u(\partial_{xy}u + \delta^2 \partial_{xx}v) \\ & + v(\partial_{yy}u + \delta^2 \partial_{xy}v) + 2\partial_x u(\partial_y u - \delta^2 \partial_x v)] \end{aligned} \quad (24)$$

$$\tau_{yy} = 2\{\partial_y v - \delta De(1-r)[\partial_{yt}v + u\partial_{xy}v + v\partial_{yy}v - (\partial_y u + \delta^2 \partial_x v)\partial_x v - 2(\partial_y v)^2]\}. \quad (25)$$

Obviously, in the weak viscoelasticity limit, a single parameter  $M = De(1-r)$  could be introduced to characterize the overall effect of viscoelasticity. And the time constant ratio  $r$  always acts to alleviate the impact of the viscoelasticity in this case. Moreover, the above expressions (23)–(25) for the stresses are actually the same as those for the Walters' liquid B'' [36].

The pressure  $p$  in the streamwise momentum equation (13) is determined by integrating the cross-streamwise momentum equation (14) from  $y$  to  $h$  and inserting the boundary condition (21), which yields

$$p = \frac{3 \cot \theta}{\text{Re}}(h-y) - \frac{\delta}{\text{Re}} \partial_x u - \frac{\delta}{\text{Re}} (\partial_x u)|_{y=h} - \delta^2 \frac{3We}{\text{Re}} \partial_{xx} h. \quad (26)$$

In Eq. (26) we have dropped terms of higher order than  $O(\delta)$ , since it would be multiplied with  $\delta$  in Eq. (13) [the surface tension term is kept with  $We$  assumed to be of  $O(1/\delta)$  or larger].

Then we integrate Eq. (12) over the film thickness and apply the no-slip (18) and kinematic conditions (19). In accordance with the Galerkin method,  $b$  is chosen as a weighted function and multiplied with Eq. (13) from  $y = 0$  to  $y = h$ , we finally obtain the following coupled equations for  $h$  and  $q$ :

$$h_t + q_x = 0, \quad (27)$$

$$\begin{aligned} q_t + \left( \frac{9q^2}{7h} + \frac{5 \cot \theta}{4\text{Re}} h^2 \right)_x = & \frac{q}{7h} q_x + \frac{5}{2\delta \text{Re}} \left( h - \frac{q}{h^2} \right) + \frac{5\delta^2 We}{2\text{Re}} h h_{xxx} \\ & + \frac{\delta}{\text{Re}} \left( \frac{9}{2} q_{xx} - \frac{9}{2h} q_x h_x + \frac{4q}{h^2} h_x^2 - \frac{6q}{h} h_{xx} \right) \\ & + \frac{5De(1-r)}{2\text{Re}h^4} (h^2 q_t + 6hq q_x - 6q^2 h_x), \end{aligned} \quad (28)$$

where the subscripts  $x$  and  $t$  denote the corresponding partial derivatives hereinafter except for those in stress components. Equations (27)–(28) constitute a second-order WRIBL model for a thin falling film with weak viscoelasticity. We note that by setting  $De = 0$  or  $r = 1$ , it recovers the original case proposed by Ruyer-Quil and Manneville [18] for a Newtonian fluid.

### III. LINEAR STABILITY ANALYSIS

A standard normal mode approach is adopted to study the linear stability of the film. For the WRIBL equations (27)–(28), we impose small disturbance on the basic flow so that

$$(h, q) = (1, 1) + (\hat{h}, \hat{q})\exp(ikx + \omega t) + \text{c.c.}, \quad (29)$$

where c.c. represents the complex conjugate of the second term. Substituting Eq. (29) into Eqs. (27)–(28) and linearizing the resulting equations, one obtains a dispersion equation in the form

$$\begin{vmatrix} \Psi_{11} & \Psi_{12} \\ \Psi_{21} & \Psi_{22} \end{vmatrix} = 0, \quad (30)$$

where  $\Psi_{11}$ – $\Psi_{22}$  are expressed by

$$\begin{aligned} \Psi_{11} &= \omega, & \Psi_{12} &= ik, \\ \Psi_{21} &= \frac{-105 + 35iWe\delta^3k^3 - 84\delta^2k^2 - i\delta k[18\text{Re} - 35 \cot \theta - 210De(1-r)]}{14\delta\text{Re}}, \\ \Psi_{22} &= \frac{35 + 63\delta^2k^2 - \delta De(1-r)(210ik + 35\omega) + \delta\text{Re}(34ik + 14\omega)}{14\delta\text{Re}}. \end{aligned} \quad (31)$$

Letting the complex frequency  $\omega = \omega_r + i\omega_i$ , it is easy for us to evaluate the temporal growth rate  $\omega_r$  and the neutral stability curves, whereby one can readily determine the critical Reynolds number as

$$\text{Re}_{\text{crit}} = \frac{5}{6} \cot \theta - \frac{5}{2} De(1-r). \quad (32)$$

which decreases as the viscoelasticity parameter  $M = De(1-r)$  becomes larger, thus implying a destabilizing impact of the viscoelastic effect. Note that Eq. (32) agrees with some early studies on viscoelastic films [27–29].

On the other hand, we also make an effort to solve the full linearized equations of Eqs. (12)–(21) as a check for Eq. (30). Imposing a small disturbance

$$(u', v', p', h', \tau'_{xx}, \tau'_{xy}, \tau'_{yy}) = (\hat{u}, \hat{v}, \hat{p}, \hat{h}, \hat{\tau}_{xx}, \hat{\tau}_{xy}, \hat{\tau}_{yy})\exp(ikx + \omega t) + \text{c.c.}, \quad (33)$$

an ordinary differential equation eigenvalue problem emerges with  $\omega$  being the eigenvalue. We employ a Chebyshev spectral collocation method to solve it, which is a well-known technique and has been widely used in hydrodynamic stability problems [44]. After discretization based on polynomial interpolation with Chebyshev points, the system is converted into a generalized eigenvalue problem

$$\mathbf{A}\mathbf{s} = \omega\mathbf{B}\mathbf{s}, \quad (34)$$

where  $\mathbf{A}$  and  $\mathbf{B}$  are square matrices with  $\mathbf{s}$  being a column vector containing the values of  $\hat{u}$ ,  $\hat{v}$ ,  $\hat{p}$ ,  $\hat{\tau}_{xx}$ ,  $\hat{\tau}_{xy}$ ,  $\hat{\tau}_{yy}$ , and  $\hat{h}$  at the collocation points. The computer program is established within the framework of a universal software package developed before [45].

Figure 2 depicts the influence of the Deborah number on the film instability. As  $De$  becomes larger, the temporal growth rate and the cut-off wave number  $k_c$  increases; while the instability threshold decreases as shown in Fig. 2(b), which is also indicated by Eq. (32). And the wave speed decreases in the meantime, which implies that the viscoelasticity strengthens the dispersion effect of the waves. However, an opposite impact of the viscoelasticity on  $k_c$  is revealed by the full equations, i.e., the cut-off wave number starts to decrease with  $De$ , especially for larger Reynolds numbers.

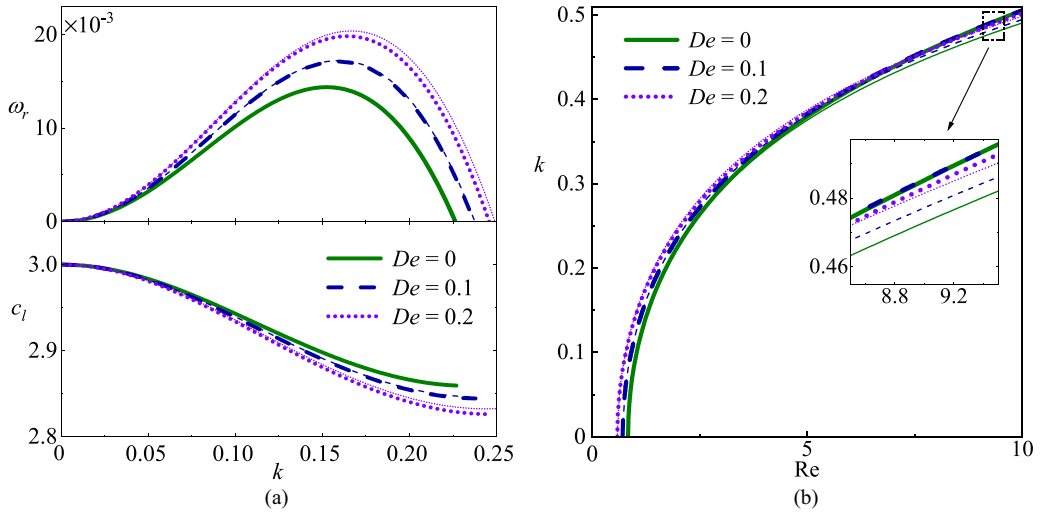


FIG. 2. Influence of the Deborah number on (a) temporal growth rate  $\omega_r$  and wave speed  $c_l = -\omega_i/k$  at  $Re = 2$ ; and (b) neutral stability curves on the  $(Re, k)$  plane when  $We = 20$ ,  $\theta = \pi/4$ , and  $r = 0.5$ . Thick and thin lines correspond to the full equations and WRIBL, respectively (same notation is adopted in Figs. 3 and 4).

Actually, this stabilizing effect of viscoelasticity would be more prominent when  $De$  takes larger values, as the growth rate would decrease remarkably with  $De$  except for very long waves [27]. We note that this stabilizing effect is not captured by the present WRIBL model, which could be attributed to its long-wave nature as well as the weak viscoelasticity approximation applied in the formulation. Apart from that, a nice agreement is observed between WRIBL and full equations, especially for long waves and relatively small Reynolds numbers.

Presented in Fig. 3 is the impact of the time constant ratio  $r$ . Compared with the Deborah number, an almost opposite effect could be found for the temporal growth rates, wave speeds, and the

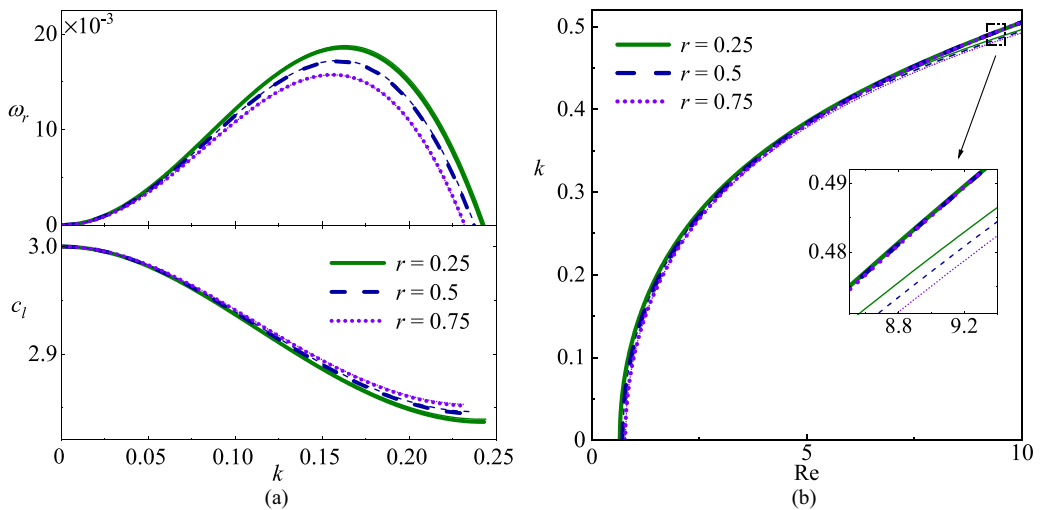


FIG. 3. Influence of the time constant ratio on (a) temporal growth rate  $\omega_r$  and wave speed  $c_l = -\omega_i/k$  at  $Re = 2$ ; and (b) neutral stability curves on the  $(Re, k)$  plane when  $We = 20$ ,  $\theta = \pi/4$ , and  $De = 0.1$ .

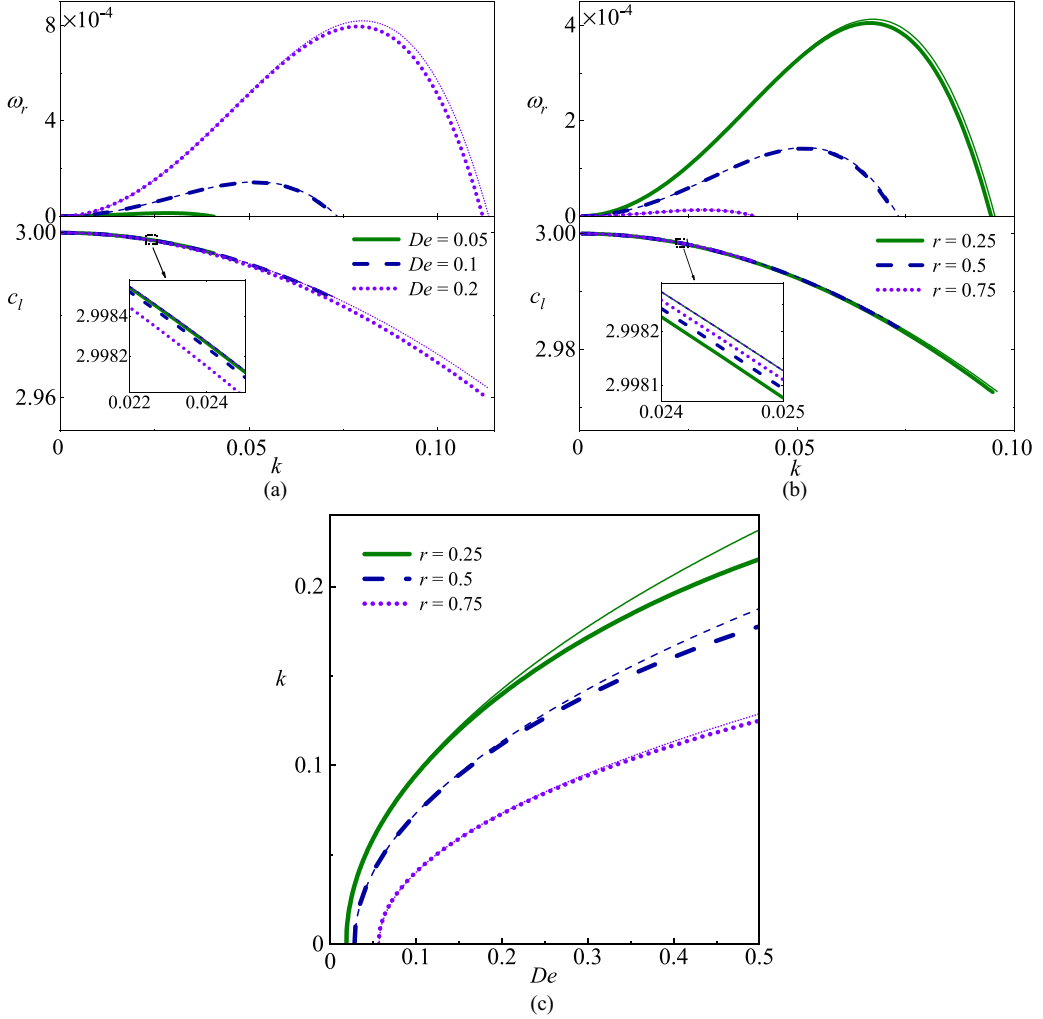


FIG. 4. Results of elastic instability when  $Re = 0$ ,  $We = 20$ ,  $\theta = 18\pi/37$ . (a) and (b) temporal growth rate  $\omega_r$  and wave speed  $c_l = -\omega_i/k$  at different  $De$  and  $r$ ; (c) neutral stability curves on the  $(De, k)$  plane.

cut-off wave numbers when increasing  $r$ , which means that the effect of viscoelasticity is basically weakened as  $r$  becomes greater. This result is evident since the viscoelasticity parameter  $M$  increases with  $De$  while decreases with  $r$ . And as  $r \rightarrow 1$ , a Newtonian film would be eventually recovered, which is anticipated to be less unstable than those with weak viscoelastic effect.

As stated in previous studies [27,31], purely elastic instability is possible to dominate the film flow at vanishing Reynolds numbers, which could also be anticipated from Eq. (32). In fact, setting  $Re = 0$  in Eq. (32), the critical value of the Deborah number for purely elastic instability is

$$De_{\text{crit}} = \frac{\cot \theta}{3(1-r)}. \quad (35)$$

Figure 4 displays the results of this elastic instability for a nearly vertical plane. Obviously, both the growth rates and cut-off wave numbers increase remarkably by the viscoelasticity of the fluid; and a minor reduction is observed for the wave speed meanwhile. Also, the unstable region on



$(De, k)$  plane expands when  $r$  increases. However, the growth rates of the elastic instability are much smaller than those in Figs. 2 and 3. Note that WRIBL well reproduces the results of full equations for small Deborah numbers; while the deviation gradually arises when  $De$  becomes greater and the weak viscoelasticity approximation starts to be violated.

In addition, by letting  $\omega = -kc$ , the model dispersion relation (30) can be rewritten in the form

$$i(c - c_k) + \Omega(\text{Re})k(c - c_{d+})(c - c_{d-}) = 0, \quad (36)$$

which corresponds to a wave hierarchy considered by Whitham [46] with  $\Omega(\text{Re}) = \text{Re}(2 - 5M_0)/(9k^2 + 5)$  and  $M_0 = M/\text{Re}$  being a reduced viscoelastic parameter. Equation (36) could be seen as a two-part combination of wave dispersion relation with a phase shift of  $\pi/2$ . The first kind of waves are referred to as kinematic waves which dominate in the inertialess limit  $\Omega(\text{Re}) \rightarrow 0$ , where the velocity field and the flow rate are slaved to the evolution of the film height as implied by the kinematic boundary condition (19). And these waves travel at the speed

$$c_k = \frac{3(4k^2 + 5)}{9k^2 + 5}, \quad (37)$$

which is three times the average velocity of the basic flow in the long-wave limit, with the second-order viscous effect playing a dispersive role there as underlined by Ruyer-Quil *et al.* [47]. On the other hand, the second kind are dynamic waves that are enhanced by the inertial effects and propagate at speeds

$$c_{d\pm} = \frac{1}{2} \left[ F \pm \sqrt{F^2 - G + \frac{(\cot \theta + Wek^2)}{\text{Re}} I} \right] \quad (38)$$

with

$$F = \frac{34 - 210M_0}{14 - 35M_0}, \quad G = \frac{72 - 840M_0}{14 - 35M_0}, \quad I = \frac{20}{2 - 5M_0}. \quad (39)$$

These waves relate to the perturbation of the momentum, pressure and surface tension effect induced by the free-surface deformation. Apparently, the dispersion of dynamic waves is caused by the surface tension. In the framework of the Whitham wave hierarchy, the instability results from the competition of the two kind of waves and the stability condition could be expressed as

$$c_{d-} \leq c_k \leq c_{d+}. \quad (40)$$

Figure 5 illustrates the dynamic wave speeds as functions of the generalized Froude number  $Fr^2 = (\cot \theta + Wek^2)/\text{Re}$ . The dynamic waves travel at a lower speed close to the free-surface base velocity, which are actually associated with capillary-gravity waves advected by the fluid there. As noted by Smith [12], a key factor for the primary instability of the film lies in the fact that the kinematic waves travel faster than any fluid particle. In the current situation, the instability happens when  $c_k$  is larger than  $c_{d+}$ . And though the speed of kinematic waves is not altered by the viscoelasticity from Eq. (37), the dynamic waves are decelerated by the viscoelastic effect, which reduces the gap between the speeds of kinematic and dynamic waves and thus plays a destabilizing role.

#### IV. TRAVELING WAVE SOLUTIONS

Initial disturbances generally evolve into steady traveling waves on the films which propagate at a constant speed  $c$  and wave shape, as reported by many authors [48,49]. And in this section, the WRIBL equations (27)–(28) are utilized to determine these traveling wave solutions. First, we introduce a moving frame  $\xi = x - ct$  and Eq. (27) writes

$$-ch' + q' = 0, \quad (41)$$

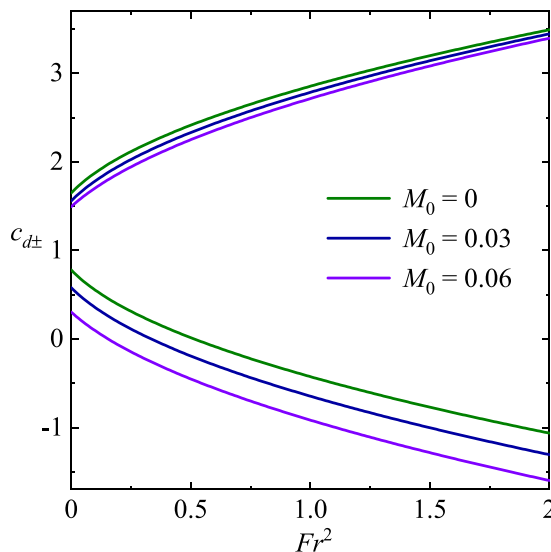


FIG. 5. Effect of the reduced viscoelastic parameter  $M_0$  on the dynamic wave speeds  $c_{d\pm}$ .

where a prime denotes the derivative with respect to  $\xi$ . Integrating Eq. (41) yields  $q = ch + q_0$  with  $q_0$  being an integral constant. Substituting this into Eq. (28) we obtain the model equation in the moving frame

$$A_1 h''' + A_2 h'' + A_3 h'^2 + A_4 h' + A_5 = 0 \quad (42)$$

with  $A_1 - A_5$  given in the Appendix. And a closed flow condition is imposed with

$$\frac{1}{L} \int_0^L h d\xi = 1, \quad (43)$$

which requires that the waves carry the same mass as the basic uniform film of same periodicity with wavelength  $L = 2\pi/k$ . We seek traveling wave solutions to Eqs. (42)–(43) by a continuation software package Auto07p [50], where an initial guess of the branches is obtained from the neutral stability solutions.

Steady traveling waves correspond to limit cycles in the phase space in the view of a dynamic system. Figure 6 displays the influence of the viscoelasticity on the bifurcation diagram. The fast-wave  $\gamma_2$  family bifurcates from the neutral stability solution through a Hopf bifurcation; while the slow-wave  $\gamma_1$  family emerges from the  $\gamma_2$  family through a period-doubling bifurcation. According to Scheid *et al.* [51], this bifurcation behavior would be reversed when  $\text{Re}$  takes sufficiently larger value and the viscous diffusion is small; while it is not altered by a weak viscoelastic effect considered here. It is obvious that the viscoelasticity decelerates the slow waves and accelerates the fast waves and thus inducing an additional dispersion effect, which is consistent with the result of linear stability analysis in Figs. 2 and 3. While the gap between the maximum and minimum free-surface amplitudes  $\Delta h_m$  is amplified for both  $\gamma_1$  and  $\gamma_2$  waves at the same time. We further depict the profiles of two kinds of waves in Fig. 7. The fast  $\gamma_2$  waves are typically one large hump preceded by a series of small decaying capillary ripples; and the slow  $\gamma_1$  waves consist of one trough followed by capillary ripples. Specially, for fast waves the amplitude of the main hump is magnified by the viscoelastic effect and the height of the flat portion of the waves slightly decreases owing to the conservation of mass, showing a tendency to strengthen the free-surface deformation. Similar impact is observed for slow waves where the amplitudes of both troughs and capillary ripples are enlarged.

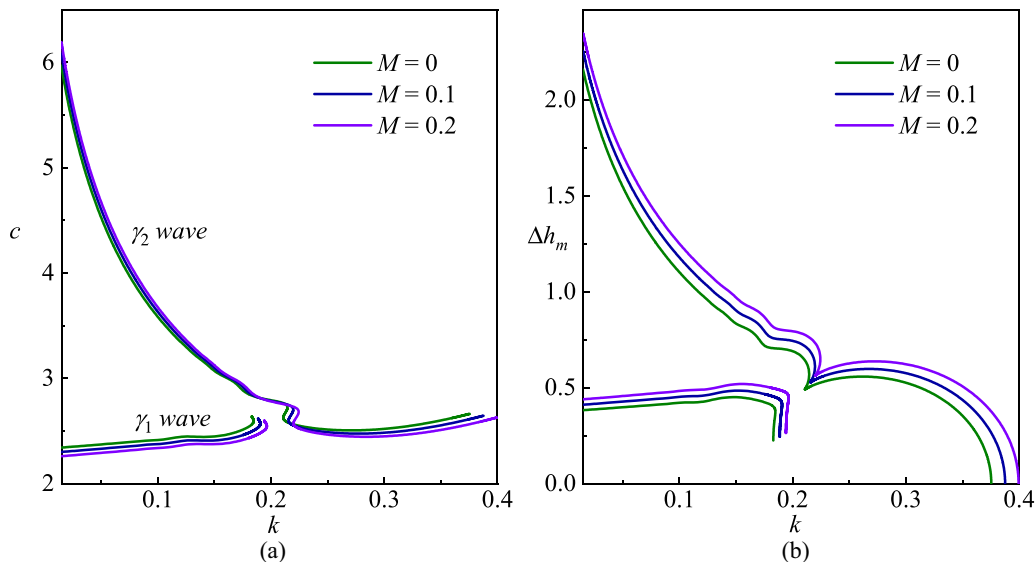


FIG. 6. (a) The speed of the traveling waves and (b) the gap between the maximum and minimum amplitudes  $\Delta h_m = h_{\max} - h_{\min}$  at different viscoelastic parameters when  $\theta = \pi/4$ ,  $\text{Re} = 5$ , and  $\text{We} = 20$ .

The characteristics of  $\gamma_2$  waves are explored in Fig. 8, since only one-hump waves could be obtained during the simulation [15]. As the Reynolds number increases, the wave speed  $c$  first grows rapidly and slowly decreases from a local maximum at higher  $\text{Re}$ ; whereas a similar trend is found for the amplitude gap  $\Delta h_m$ , except for a nearly plateau region at larger  $\text{Re}$ . According to Ooshida [52], the first regime is referred to as the drag-gravity regime where the inertia effect is relatively weak and thus the viscous drag and gravity are dominating. The second regime is called the drag-inertia regime where the inertia effect governs the film flow. We can see that viscoelasticity results in an amplification of both the speed and amplitude of the waves in the two regimes.

## V. NONLINEAR SIMULATIONS

We perform time-dependent simulations based on the model equations (27)–(28) under periodic boundary conditions in this section. Spatial derivatives are calculated using the Fourier spectral

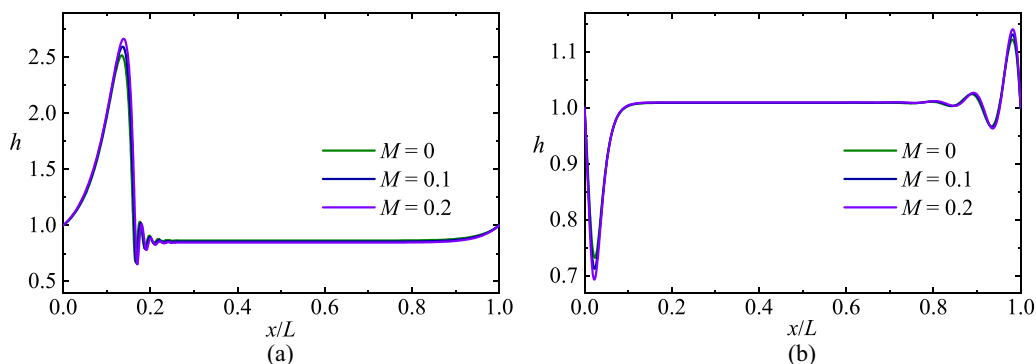


FIG. 7. Wave profiles of the film thickness  $h$ : (a) fast  $\gamma_2$  family and (b) slow  $\gamma_1$  family at different viscoelastic parameters when  $k = 0.03$ . Other parameters are the same with those in Fig. 6.

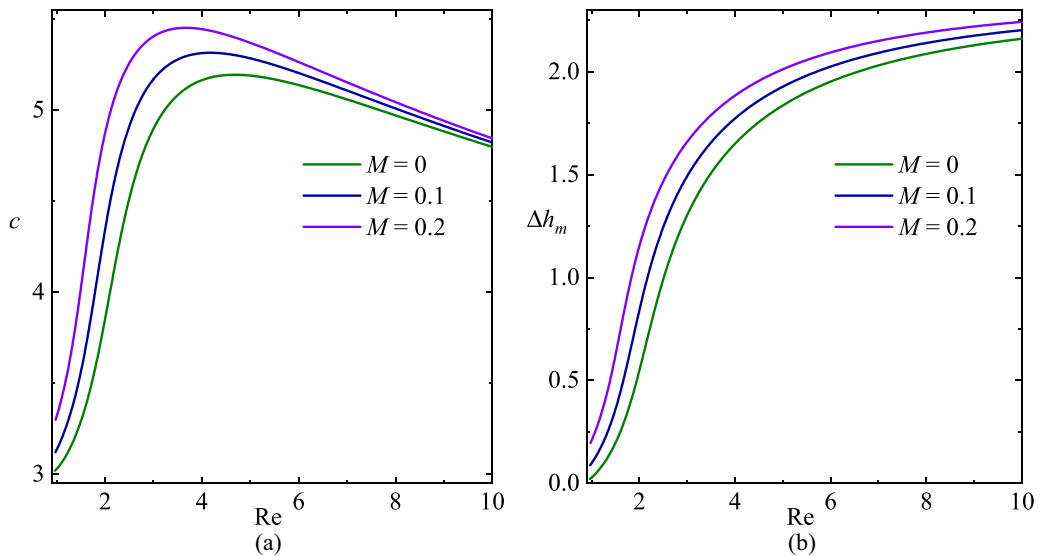


FIG. 8. (a) The speed and (b) the amplitude gap at different viscoelastic parameters when  $\theta = \pi/4$ ,  $We = 20$ , and  $k = 0.03$ .

method and 128–512 nodes are generally enough for most cases with sufficient accuracy. The solution is advanced in time through the MATLAB routine ode45. An initial disturbance is imposed on the basic flow

$$h(x, 0) = 1 + \epsilon \sin(kx). \quad (44)$$

Moreover, a perturbation energy function is defined

$$E = \frac{1}{L} \int_0^L (h - 1)^2 dx. \quad (45)$$

We first monitor the evolution of the initial disturbance at different Reynolds numbers. It can be seen that results in Fig. 9 agree with linear stability analysis. The perturbation energy  $E$  continues to decay when Reynolds number is below the threshold value  $Re_{\text{crit}}$  and the film gradually approaches the basic uniform state; while for  $Re > Re_{\text{crit}}$  in Fig. 9,  $E$  first experiences a growing process and finally saturates at a finite value when steady permanent waves are typically formed on the free surface. This further enables us to evaluate the instability threshold and the result is compared with the linear stability analysis in Fig. 10. Nice agreement is observed between nonlinear simulations and linear predictions of both WRIBL and full equations. Effects of the viscoelasticity on the film evolution are illustrated in Fig. 11. As  $M$  increases, the perturbation energy grows faster in the initial stage and saturates at a higher value eventually. And the profiles of the waves formed in the final stage are quite similar to each other, with a larger amplitude of the main hump as the viscoelastic effect becomes stronger, which is consistent with the results in Fig. 7.

## VI. CONCLUSION

This paper considers the gravity-driven flow of a thin film of Oldroyd-B fluid down an incline. A weighted residual integral boundary layer model (WRIBL) is derived to study long-wave instability of the film. Linear stability analysis is conducted by a normal mode approach, where the viscoelastic effect is found to destabilize the film and decrease the speed of linear waves. Results of the WRIBL model agree with the full linearized equations satisfactorily for Reynolds numbers near

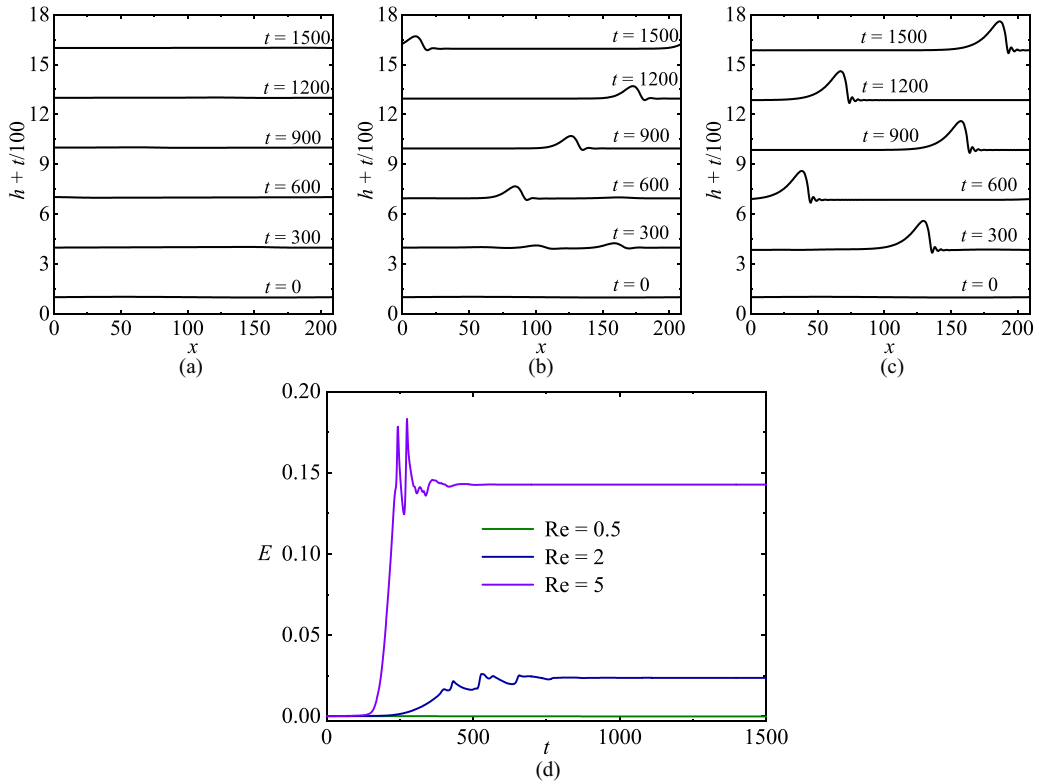


FIG. 9. Wave evolution (a)  $Re = 0.5$ , (b)  $Re = 2$ , and (c)  $Re = 5$ . (d) Evolution of perturbation energy  $E$ . The other parameters are  $\theta = \pi/4$ ,  $We = 20$ ,  $M = 0.1$ , and  $k = 0.03$ .

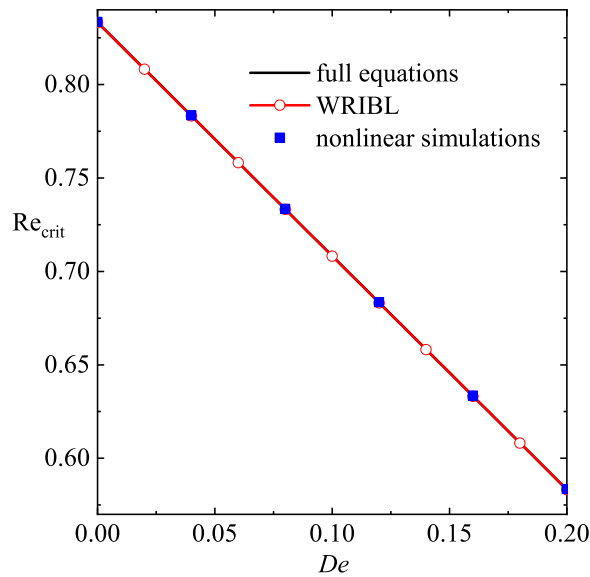


FIG. 10. Comparison of the critical Reynolds number when  $\theta = \pi/4$ ,  $We = 20$ ,  $r = 0.5$ .

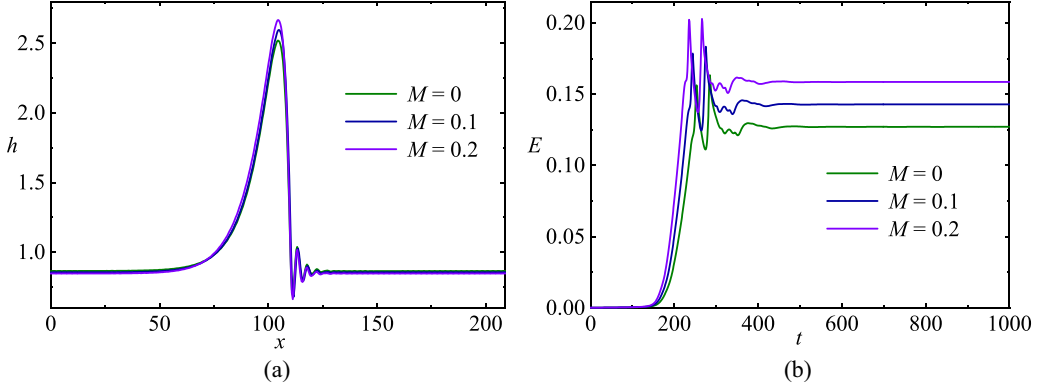


FIG. 11. Wave evolution at different viscoelastic numbers: (a) wave profiles at  $t = 1000$  and (b) evolution of perturbation energy  $E$  when  $\theta = \pi/4$ ,  $\text{Re} = 5$ ,  $\text{We} = 20$ , and  $k = 0.03$ .

the criticality and the purely elastic instability is also identified when  $\text{Re}$  vanishes. While the stabilizing impact of the viscoelasticity at moderate Reynolds numbers revealed by full equations is not captured by the present model, which is due to the weak viscoelasticity approximation. A further exploration on the dispersion relation is carried out within the framework of the Whitham wave hierarchy. The viscoelastic effect acts to promote the speed of dynamic waves with no influence left on that of the kinematic waves, thus enhancing the instability. Traveling wave solutions are obtained from the model equations. The speed gap between fast and slow waves is augmented by the viscoelasticity, which results in an additional dispersion effect. And the deformation of the free surface is also amplified as the viscoelastic number increases. Nonlinear simulations are performed to investigate the temporal evolution of the film, which support the linear prediction of the instability threshold. After a transient growing process, steady permanent waves are formed in the final stage. And the viscoelasticity strengthens the surface deformation and the perturbation energy of these traveling waves.

#### ACKNOWLEDGMENTS

This work was supported by the China's National Natural Science Funds for Distinguished Young Scholar (Grant No. 11525207) and China's National Natural Science Foundation (Grants No. 11922201 and No. 11672025).

#### APPENDIX: COEFFICIENTS OF THE MODEL EQUATION IN THE MOVING FRAME

The coefficients  $A_1 - A_5$  in Eq. (42) are

$$\begin{aligned}
 A_1 &= -\frac{5\delta^2 \text{We}}{2\text{Re}} h, & A_2 &= \frac{3\delta(ch + 4q_0)}{2\text{Re}h}, & A_3 &= \frac{\delta(ch - 8q_0)}{2\text{Re}h^2}, \\
 A_4 &= \frac{35 \cot \theta h^5 + 2c^2 \text{Re}h^4 - 2c\text{Re}q_0 h^3 + (35Mc^2 - 18\text{Re}q_0^2)h^2 + 210Mq_0(ch + q_0)}{14\text{Re}h^4}, \\
 A_5 &= -\frac{5}{2\delta\text{Re}h^2} (h^3 - ch - q_0).
 \end{aligned} \tag{A1}$$

[1] W. M. Salvagnini and M. E. S. Taqueda, A falling-film evaporator with film promoters, *Ind. Eng. Chem. Res.* **43**, 6832 (2004).

- [2] S. J. Weinstein and K. J. Ruschak, Coating flows, *Annu. Rev. Fluid Mech.* **36**, 29 (2004).
- [3] S. Shine and S. Nidhi, Review on film cooling of liquid rocket engines, *Propul. Power Res.* **7**, 1 (2018).
- [4] H. Chang, Wave evolution on a falling film, *Annu. Rev. Fluid Mech.* **26**, 103 (1994).
- [5] A. Oron, S. H. Davis, and S. G. Bankoff, Long-scale evolution of thin liquid films, *Rev. Mod. Phys.* **69**, 931 (1997).
- [6] R. V. Craster and O. K. Matar, Dynamics and stability of thin liquid films, *Rev. Mod. Phys.* **81**, 1131 (2009).
- [7] S. Kalliadasis, C. Ruyer-Quil, B. Scheid, and M. G. Velarde, *Falling Liquid Films* (Springer London, 2012).
- [8] P. L. Kapitza and S. P. Kapitza, Wave flow of thin layers of viscous liquids. Part III. Experimental research of a wave flow regime, *Zh. Eksp. Teor. Fiz.* **19**, 105 (1949).
- [9] T. B. Benjamin, Wave formation in laminar flow down an inclined plane, *J. Fluid Mech.* **2**, 554 (1957).
- [10] C.-S. Yih, Stability of liquid flow down an inclined plane, *Phys. Fluids* **6**, 321 (1963).
- [11] J. Liu, J. D. Paul, and J. P. Gollub, Measurements of the primary instabilities of film flows, *J. Fluid Mech.* **250**, 69 (1993).
- [12] M. K. Smith, The mechanism for the long-wave instability in thin liquid films, *J. Fluid Mech.* **217**, 469 (1990).
- [13] C. Ruyer-Quil, N. Kofman, D. Chasseur, and S. Mergui, Dynamics of falling liquid films, *Eur. Phys. J. E* **37**, 1 (2014).
- [14] D. J. Benney, Long waves on liquid films, *J. Math. Phys.* **45**, 150 (1966).
- [15] A. Pumir, P. Manneville, and Y. Pomeau, On solitary waves running down an inclined plane, *J. Fluid Mech.* **135**, 27 (1983).
- [16] V. Y. Shkadov, Wave flow regimes of a thin layer of viscous fluid subject to gravity, *Fluid Dyn.* **2**, 29 (1967).
- [17] C. Ruyer-Quil and P. Manneville, Modeling film flows down inclined planes, *Eur. Phys. J. B* **6**, 277 (1998).
- [18] C. Ruyer-Quil and P. Manneville, Improved modeling of flows down inclined planes, *Eur. Phys. J. B* **15**, 357 (2000).
- [19] A. Pereira and S. Kalliadasis, Dynamics of a falling film with solutal marangoni effect, *Phys. Rev. E* **78**, 036312 (2008).
- [20] S. J. D. D'Alessio, J. P. Pascal, and H. A. Jasmine, Instability in gravity-driven flow over uneven surfaces, *Phys. Fluids* **21**, 062105 (2009).
- [21] A. Samanta, C. Ruyer-Quil, and B. Goyeau, A falling film down a slippery inclined plane, *J. Fluid Mech.* **684**, 353 (2011).
- [22] Q.-F. Fu, T. Hu, and L.-J. Yang, Instability of a weakly viscoelastic film flowing down a heated inclined plane, *Phys. Fluids* **30**, 084102 (2018).
- [23] S. J. D. D'Alessio, J. P. Pascal, E. Ellaban, and C. Ruyer-Quil, Marangoni instabilities associated with heated surfactant-laden falling films, *J. Fluid Mech.* **887**, A20 (2020).
- [24] R. B. Bird, R. C. Armstrong, and O. Hassager, *Dynamics of Polymeric Liquids, Volume I: Fluid Mechanics*, 2nd ed. (A Wiley-Interscience Publication, John Wiley & Sons, 1987).
- [25] J. Dunn and K. Rajagopal, Fluids of differential type: Critical review and thermodynamic analysis, *Int. J. Eng. Sci.* **33**, 689 (1995).
- [26] A. S. Gupta, Stability of a visco-elastic liquid film flowing down an inclined plane, *J. Fluid Mech.* **28**, 17 (1967).
- [27] E. S. Shaqfeh, R. G. Larson, and G. H. Fredrickson, The stability of gravity driven viscoelastic film-flow at low to moderate reynolds number, *J. Non-Newtonian Fluid Mech.* **31**, 87 (1989).
- [28] A. S. Gupta and L. Rai, Stability of an elastico-viscous liquid film flowing down an inclined plane, *Math. Proc. Cambridge Philos. Soc.* **63**, 527 (1967).
- [29] W. Lai, Stability of an elastico-viscous liquid film flowing down an inclined plane, *Phys. Fluids* **10**, 844 (1967).
- [30] S. W. Joo, The stability and nonlinear flow developments of a viscoelastic draining film with shear thinning, *J. Non-Newtonian Fluid Mech.* **51**, 125 (1994).

- [31] F. Kang and K. P. Chen, Nonlinear elastic instability of gravity-driven flow of a thin viscoelastic film down an inclined plane, *J. Non-Newtonian Fluid Mech.* **57**, 243 (1995).
- [32] J. Tihon and O. Wein, Stability of the viscoelastic film flow down an inclined plane, in *Progress and Trends in Rheology V* (Steinkopff, Heidelberg, 1998), pp. 165–166.
- [33] H. I. Andersson and E. N. Dahl, Gravity-driven flow of a viscoelastic liquid film along a vertical wall, *J. Phys. D* **32**, 1557 (1999).
- [34] B. Uma and R. Usha, Interfacial phase change effects on the stability characteristics of thin viscoelastic liquid film down a vertical wall, *Int. J. Eng. Sci.* **42**, 1381 (2004).
- [35] S. Saprykin, R. J. Koopmans, and S. Kalliadasis, Free-surface thin-film flows over topography: Influence of inertia and viscoelasticity, *J. Fluid Mech.* **578**, 271 (2007).
- [36] N. Amatoousse, H. A. Abderrahmane, and N. Mehidi, Traveling waves on a falling weakly viscoelastic fluid film, *Int. J. Eng. Sci.* **54**, 27 (2012).
- [37] L. A. Davalos-Orozco, Stability of thin viscoelastic films falling down wavy walls, *Interfacial Phenom. Heat Transfer* **1**, 301 (2013).
- [38] A. Sharma, P. K. Ray, and D. T. Papageorgiou, Dynamics of gravity-driven viscoelastic films on wavy walls, *Phys. Rev. Fluids* **4**, 063305 (2019).
- [39] D. Pettas, G. Karapetsas, Y. Dimakopoulos, and J. Tsamopoulos, Viscoelastic film flows over an inclined substrate with sinusoidal topography. I. Steady state, *Phys. Rev. Fluids* **4**, 083303 (2019).
- [40] D. Pettas, G. Karapetsas, Y. Dimakopoulos, and J. Tsamopoulos, Viscoelastic film flows over an inclined substrate with sinusoidal topography. II. Linear stability analysis, *Phys. Rev. Fluids* **4**, 083304 (2019).
- [41] D. F. James, Boger fluids, *Annu. Rev. Fluid Mech.* **41**, 129 (2009).
- [42] S. Kalliadasis, E. A. Demekhin, C. Ruyer-Quil, and M. G. Velarde, Thermocapillary instability and wave formation on a film falling down a uniformly heated plane, *J. Fluid Mech.* **492**, 303 (2003).
- [43] Z.-Q. Zhou, J. Peng, Y.-J. Zhang, and W.-L. Zhuge, Viscoelastic liquid film flowing down a flexible tube, *J. Fluid Mech.* **802**, 583 (2016).
- [44] M. R. Khorrami, M. R. Malik, and R. L. Ash, Application of spectral collocation techniques to the stability of swirling flows, *J. Comput. Phys.* **81**, 206 (1989).
- [45] H.-Y. Ye, L.-J. Yang, and Q.-F. Fu, Spatial instability of viscous double-layer liquid sheets, *Phys. Fluids* **28**, 102101 (2016).
- [46] G. B. Whitham, *Linear and Nonlinear Waves* (John Wiley & Sons, Inc., New York, 1999).
- [47] C. Ruyer-Quil, P. Treveleyan, F. Giorgiutti-Dauphiné, C. Duprat, and S. Kalliadasis, Modelling film flows down a fibre, *J. Fluid Mech.* **603**, 431 (2008).
- [48] S. V. Alekseenko, V. Y. Nakoryakov, and B. G. Pokusaev, Wave formation on a vertical falling liquid film, *AIChE J.* **31**, 1446 (1985).
- [49] J. Liu and J. P. Gollub, Solitary wave dynamics of film flows, *Phys. Fluids* **6**, 1702 (1994).
- [50] E. J. Doedel, T. F. Fairgrieve, B. Sandstede, A. R. Champneys, Y. A. Kuznetsov, and X. Wang, *AUTO-07P: Continuation and Bifurcation Software for Ordinary Differential Equations* (2007).
- [51] B. Scheid, C. Ruyer-Quil, and P. Manneville, Wave patterns in film flows: Modelling and three-dimensional waves, *J. Fluid Mech.* **562**, 183 (2006).
- [52] T. Ooshida, Surface equation of falling film flows with moderate Reynolds number and large but finite weber number, *Phys. Fluids* **11**, 3247 (1999).